Section A-Research paper

ISSN 2063-5346

Development and Characterization of a Corrosion-Resistant Coating for Enhanced Material Protection for propulsion systems

Purshotham.P.Katti* 1
1 *Research scholor,Department of Nanotechnology ,srinivas university mangalore - 574143.Email: purshothampkatti@gmail.com
Dr.Praveen B.M*2
Department of Nanotechnology ,srinivas university mangalore -574143
Corresponding Author: Purshotham.P.Katti 1 1 *Research scholor,Department of Nanotechnology ,srinivas university mangalore - 574143.
Email: purshothampkatti@gmail.com

Received 17 January 2022, Revised 9 April 2022, Accepted 19 May 2022

Abstract:

This study focuses on the development and characterization of a novel corrosion-resistant coating combination for enhancing the durability and protection of materials in corrosive environments. The coating, comprised of Nickel Sulfate, Molybdenum Oxide, Sodium Hydroxide, Boric Acid, Ammonium Chloride, Nickel Chloride, and Sodium Chloride, was meticulously designed to impart improved resistance against corrosion. The investigation involved a comprehensive analysis of the coating's composition and its behavior under specific experimental conditions. SEM, X-ray diffraction and impedance spectroscopy techniques were employed to elucidate the coating's structural and electrochemical properties. The results highlighted the coating's ability to mitigate corrosion through its tailored composition and effective application method. This study contributes to the advancement of corrosion prevention strategies and material protection in propulsion systems [1].

DOI:10.53555/ecb/2022.11.6.39

Introduction:

Corrosion is a widespread concern that significantly impacts the longevity and integrity of materials in diverse environments. The development of effective corrosion-resistant coatings has become a pivotal area of research to combat this issue. By creating protective barriers, these coatings serve as a shield against the detrimental effects of corrosion, ensuring prolonged material lifespan and reliability [2].

In this context, the current study introduces a new corrosion-resistant coating combination tailored for enhanced protection against corrosion. The formulation of this coating involves a strategic selection of substances, each contributing unique properties to counteract the corrosive agents. The integration of Nickel Sulfate bolsters the coating's resistance, while Molybdenum Oxide promotes passivation and protection. The incorporation of Sodium Hydroxide and Boric Acid not only modulates pH levels but also encourages the development of a protective oxide layer. Additionally, Ammonium Chloride and Sodium Chloride enhance electrical conductivity and uniform deposition. By precisely controlling the concentration of each substance, a synergistic effect is achieved, amplifying the coating's overall corrosion resistance [3].

The investigation employs a combination of X-ray diffraction and impedance spectroscopy to comprehensively characterize the coating's structural and electrochemical attributes. X-ray diffraction enables the analysis of the coating's crystallographic structure and phase composition, shedding light on its fundamental properties. Impedance spectroscopy, on the other hand, provides insights into the coating's electrochemical behavior, offering a dynamic perspective on its interaction with the corrosive environment [4].

The results obtained from these analyses collectively contribute to understanding the coating's mechanism of corrosion prevention. By correlating the structural insights from X-ray diffraction with the electrochemical responses captured through impedance spectroscopy, a holistic understanding of the coating's performance is attained. This study is anticipated to advance corrosion prevention strategies and bolster the protective capabilities of materials in various industries, ranging from manufacturing to infrastructure development [5].

The investigation of this novel corrosion-resistant coating combination holds promise in revolutionizing corrosion prevention methodologies. The subsequent sections of this study delve into the experimental methodologies, results, and discussions, all aimed at unraveling the intricacies of the coating's composition and behavior. The insights gained from this study contribute to a comprehensive understanding of material behavior and corrosion mechanisms, paving the way for informed decision-making in material design and engineering applications [6].

Table 1: New Corrosion-Resistant Coating Combination

Substance	**Chemical Formula**	**Concentration (g/L)**
Nickel Sulfate	$NiSO_4•6H_2O$	40
Molybdenum Oxide	MoO_3	20
Sodium Hydroxide	NaOH	2
Boric Acid	H_3BO_3	30
Ammonium Chloride	NH_4Cl	5
Nickel Chloride	$NiCl_2$	38.84
Sodium Chloride	NaCl	5

Table 1 contains Nickel Sulfate ($NiSO_4•6H_2O$): Maintains a consistent concentration of 40 g/L to ensure a suitable nickel content in the coating.Molybdenum Oxide (MoO_3): The increased concentration of 20 g/L is aimed at enhancing the presence of molybdenum, a known promoter of passivation and improved corrosion resistance.Sodium Hydroxide (NaOH): Introduced at a minimal concentration of 2 g/L, it serves to modulate pH levels and encourage the development of a protective oxide layer.Boric Acid (H_3BO_3): The existing concentration of 30 g/L is maintained to preserve its beneficial properties for the coating.Ammonium Chloride (NH_4Cl): Introduced at a modest concentration of 5 g/L, it contributes to enhanced electrical conductivity and uniform deposition.Nickel Chloride ($NiCl_2$): Maintains the current concentration of 38.84 g/L, providing additional nickel content for corrosion protection.Sodium Chloride (NaCl): A minor concentration of 5 g/L is introduced to boost conductivity and ensure uniformity in the coating.

Figure 1: worked piece 80mm length and 20mm width

In Figure 1, an illustrative depiction showcases a workpiece with dimensions measuring 80 mm in length and 20 mm in width. Notably, a prominent feature on the surface is a coated square, clearly distinguishable. This square encompasses an area of 20 mm by 20 mm, deliberately emphasizing a specific region of interest [7].

1.1 SEM Results:

The acceleration voltage of 20.00 kilovolts (kV) represents the energy applied to particles or radiation within the instrument. This voltage is crucial in techniques like X-ray spectrometry, where higher voltages can lead to higher energy X-ray photons, enabling the analysis of heavier elements and deeper sample penetration.The probe current, measured in nanoamperes (nA), indicates the current of charged particles or radiation used for sample probing. A value of 0.00 nA suggests that, in this specific measurement, no current is applied, which can be relevant for background or reference measurements.The magnification factor of x500 means that the observed image or data is 500 times larger than the actual sample size. This parameter is common in microscopy, allowing for detailed examination at various scales.While "T3" is mentioned as a process time, it's not explicitly defined in the provided context. It likely refers to a specific step or duration within the measurement process, but the exact meaning would depend on the specific instrument and procedure.The "First" detector likely indicates the primary or initial detector used for capturing data during the measurement. Multiple detectors may be employed in some instruments for various purposes. Time signifies the actual time during which data acquisition takes place, excluding any downtime. In this case, data collection occurred continuously for 30.00 seconds. Time includes all time elapsed during the measurement, including downtime or interruptions. The recorded real-time duration for this measurement was 31.51 seconds.Dead time is the period

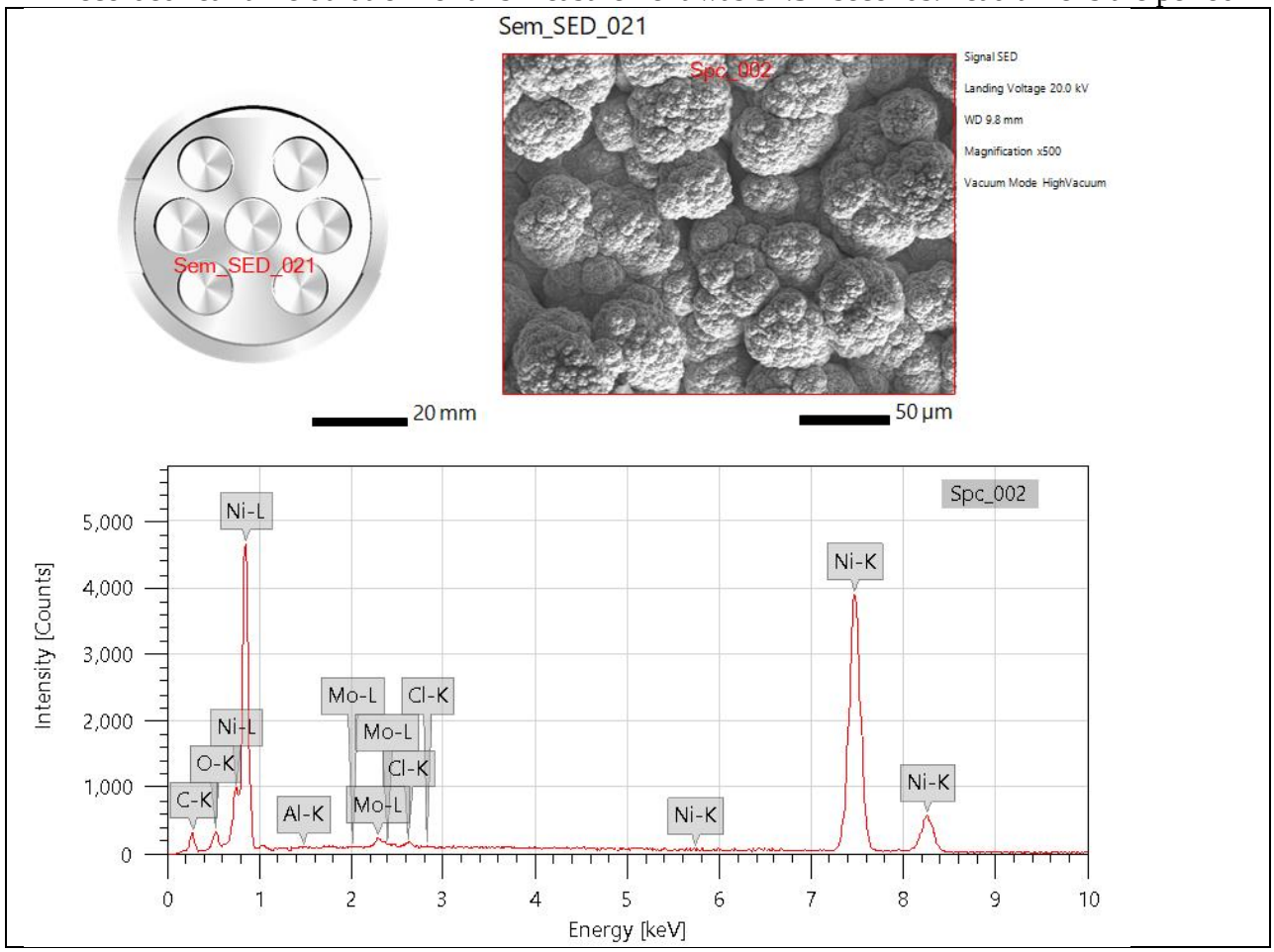

Figure 2 EDS for given solution coated

During which the detector is temporarily unable to record additional events immediately after detecting a previous event. In this instance, there was a 5- second pause in detection after each event.The count rate indicates the number of events or particles detected per second. A count rate of 6362.00 counts per second (CPS) implies that the instrument registered 6362 events per second during the measurement [11-21].

From figure 2 it is observed that :C K (Carbon):6.41% (±0.07): This represents the percentage of carbon in the sample, with an uncertainty of ±0.07%.23.94% (±0.26): This indicates the percentage of carbon when analyzed with higher energy, with an uncertainty of ±0.26%.O K (Oxygen):2.31% (±0.05): This is the percentage of oxygen in the sample, with an uncertainty of ±0.05%.6.47% (±0.14): This shows the percentage of oxygen at a higher energy level, with an uncertainty of ±0.14%.Al K (Aluminum):0.11% (±0.03): The percentage of aluminum in the sample, with an uncertainty of ±0.03%.0.18% (±0.04): The percentage of aluminum at higher energy, with an uncertainty of ±0.04%.

Cl K (Chlorine):0.33% (±0.02): The percentage of chlorine in the sample, with an uncertainty of ±0.02%.0.42% (±0.03): The percentage of chlorine at higher energy, with an uncertainty of ±0.03%.Ni K (Nickel):89.20% (±0.38): The percentage of nickel in the sample, with an uncertainty of ±0.38%.68.22% (±0.29): The percentage of nickel at higher energy, with an uncertainty of ±0.29%.Mo L (Molybdenum):1.65% (±0.06): The percentage of molybdenum in the sample, with an uncertainty of ±0.06%.0.77% (±0.03): The percentage of molybdenum at a lower energy level, with an uncertainty of ±0.03%.Total:100.00%: The sum of the percentages across all elements in the sample.Spc_002 Fitting Ratio:0.0127: This appears to be a fitting ratio or a numerical value derived from data analysis, which could be used for specific calculations or interpretations related to the analysis.

From figure 5.3 C K" refers to the X-ray emission line associated with carbon atoms when they are excited by an external energy source.In X-ray spectroscopy, the "K" line represents the innermost electron shell transitions, typically having higher energy."O K" refers to the X-ray emission line associated with oxygen atoms when they are excited.Similar to "C K," "O K" represents inner shell transitions for oxygen."Al K" denotes the X-ray emission line corresponding to aluminum atoms when they undergo X-ray excitation."Cl K" represents the X-ray emission line arising from chlorine atoms when they are excited.It is employed in analytical techniques to detect and quantify chlorine content in various samples."Ni K" signifies the X-ray emission line produced by nickel atoms upon excitation. It is been used to identify and measure the concentration of nickel in a sample."Mo L" represents an X-ray emission line associated with molybdenum atoms in the "L" shell.It is employed in X-ray fluorescence (XRF) and spectroscopy for molybdenum analysis.Molybdenum is often found in alloys and has applications in metallurgy and electronics."10 micron meter" refers to a length measurement of 10 micrometers, where a micrometer (μm) is one millionth of a meter.It is a unit of measurement used to describe small-scale dimensions, particularly in microscopy and microfabrication.
A 10-micron meter is equal to 0.01 millimeters (mm) or 10,000 nanometers (nm).

Form figure 4 EDS mapping is an indispensable tool in scientific research and various industries. Its ability to provide detailed elemental information and spatial distribution within samples aids in understanding material properties, quality control, and solving complex scientific problems. Its versatility makes it a cornerstone of analytical techniques, enabling researchers and industries to advance knowledge and technology [22-24].

Figure 5 Operates at 40 kV voltage and 30 mA current to produce X-ray radiation. This radiation interacts with the sample to initiate X-ray diffraction. The scan mode is continuous, indicating that X-ray emission remains constant throughout the scan. The standard scan speed is set to 5.00 degrees per minute. The duration time is not specified but follows standard practices. The step width of 0.01 degrees represents the angular increment between data points collected during the scan. The scan axis is $\theta/2\theta$, a common configuration in X-ray diffraction. The scan range spans from 5 to 90 degrees, encompassing the angular range over which data is collected. The Cu_K-beta_1D filter is employed to enhance specific X-ray wavelengths, improving the accuracy of analysis.

A length limiting slit of 10 mm controls the size of the diffracted X-ray beam, contributing to measurement precision.table 5.2 The DteX250(H) detector is sensitive and capable of accurately capturing diffracted X-rays. Both receiving slits (#1 and #2) are kept open, allowing the diffracted X-rays to reach the detector for analysis.This experimental setup enables X-ray diffraction analysis, a powerful technique for investigating structural changes in materials, such as those induced by corrosion processes. The specified parameters ensure precise data collection and contribute to a comprehensive understanding of material behavior and corrosion mechanisms.

The peak search method used in this analysis is the "Second derivative method" with a sigma (σ) cut-off of 3.00. This method involves identifying significant peaks in a dataset by analyzing its second derivative. By setting a sigma cut-off value, the threshold for peak detection is determined, allowing the algorithm to differentiate between true peaks and noise in the data.
In the context of the provided data, this method is employed to identify and locate peaks in a measurement, which could represent specific features or characteristics of interest. The second derivative helps in pinpointing the points of inflection or rapid changes in the original data, which often correspond to peak positions [25-26].

Additionally, the profile fitting technique has been employed with a "Split pseudo-Voigt" peak shape model. This model combines the characteristics of both Gaussian and Lorentzian peak shapes. Gaussian peaks have bell-shaped profiles, while Lorentzian peaks have more symmetric and broader profiles. The split pseudo-Voigt peak shape is a weighted combination of these two, offering a flexible model to accurately represent a wide range of peak shapes encountered in various measurements.
The fitting conditions are set to "Auto" with the option to "Refine background." This implies that the algorithm automatically adjusts the fitting parameters and optimizes the background subtraction to best fit the experimental data. The goal of the fitting process is to find the parameters that best describe the observed peaks, including their positions, heights, widths, and

shapes.

The "Second derivative method" with a sigma cut-off of 3.00 is used to identify peaks in the data, while the "Split pseudo-Voigt" peak shape model and profile fitting with automatic refinement are employed to accurately characterize these peaks figure 4.2.3. This approach ensures precise identification and quantification of features in the measurement data, contributing to a comprehensive understanding of the underlying phenomena or properties being studied [27].

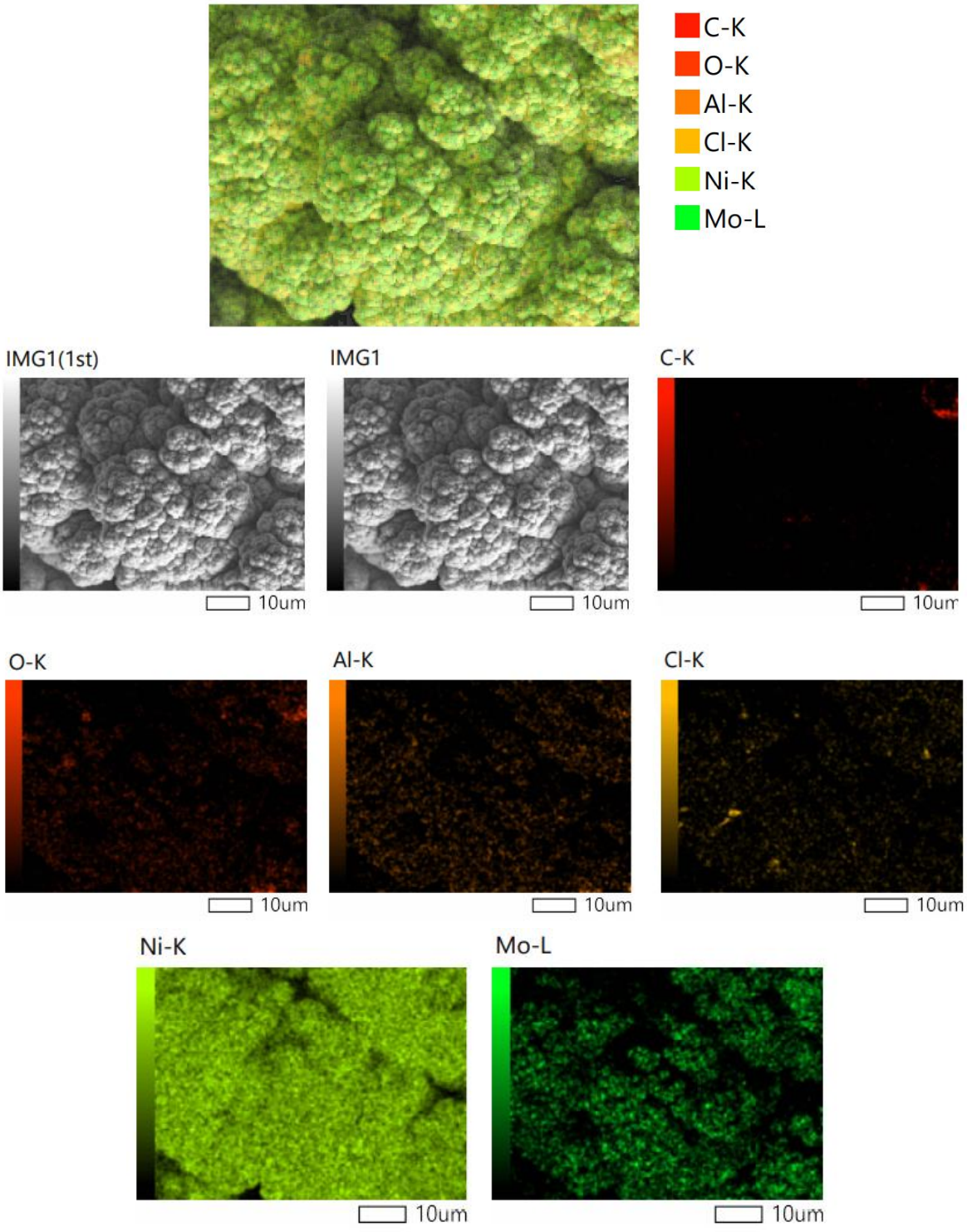

Figure 3 SEM images

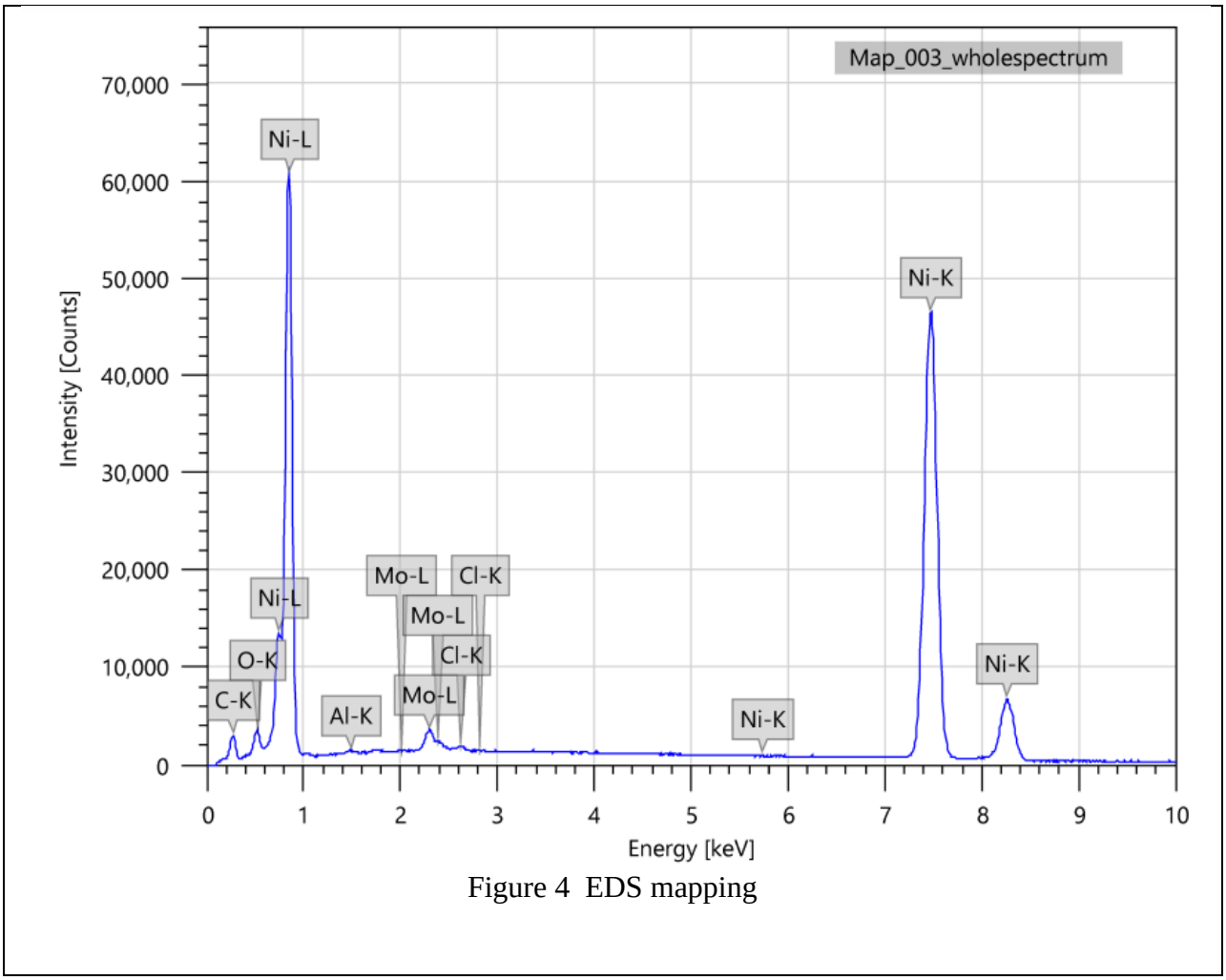

Figure 4 EDS mapping

1.2: XRD Results:

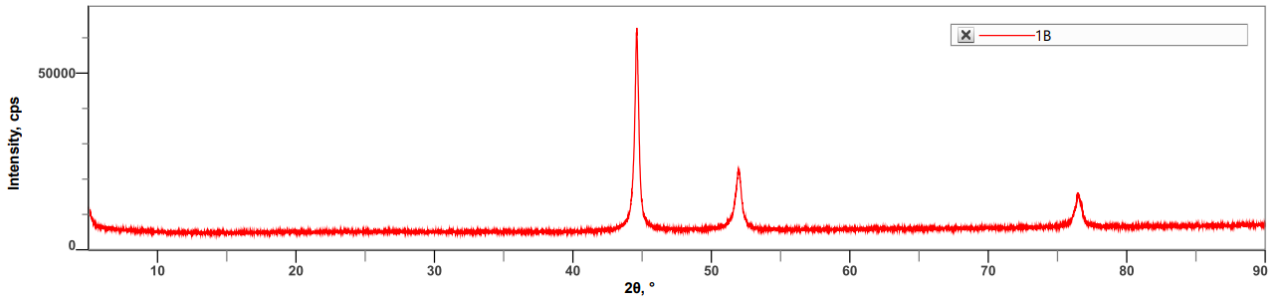

Figure 5.5: Measured Profile View

Table 2: X-Ray Diffraction Experimental Setup

Component	**Specification**	**Explanation**
X-Ray Generator	Voltage: 40 kV Current: 30 mA	Generates X-ray beam for diffraction
Scan Mode	Continuous	X-ray emission is constant during scan
Incident Primary	Scan Speed: 5.00 °/min	Rate of sample rotation during scan
	Duration Time: Standard	Time taken for each complete scan
Goniometer	Step Width: 0.01 °	Angular increment between data points
	Scan Axis: θ/2θ	Common scanning axis for X-ray diffraction
Attachment	Scan Range: 5 ~ 90 °	Angular range covered by the scan
Filter	Type: Cu_K-beta_1D	Enhances specific X-ray wavelengths
Diffracted Beam Mono	Length Limiting Slit: 10 mm	Controls size of the diffracted X-ray beam
Detector	Type: DteX250(H)	Captures diffracted X-rays with precision
Receiving Slit #1	Open	Allows diffracted X-rays to reach detector
Receiving Slit #2	Open	Further enhances X-ray beam collection

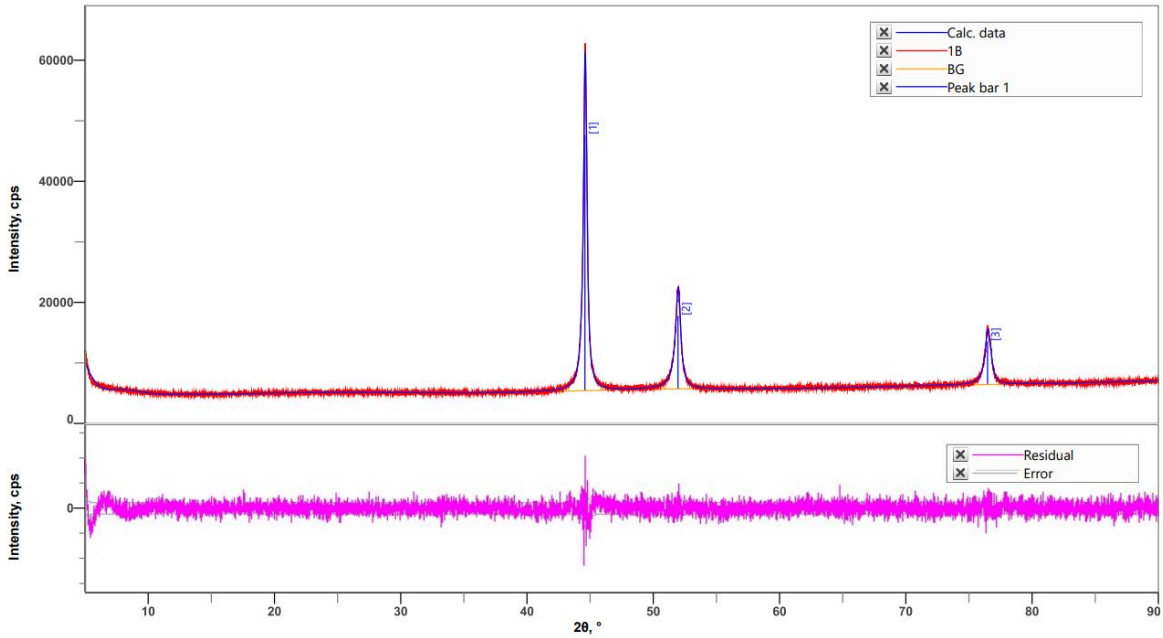

Figure 6: peak profile view

The process involved in the analysis comprises the utilization of specific techniques and parameters to extract meaningful information from the data. The key steps and their corresponding explanations, accompanied by relevant values, are outlined below:
The "Second derivative method" is employed to identify prominent peaks within the dataset. This technique analyzes the rate of change of the data points to detect significant inflection points, which often correspond to peaks. The sigma (σ) cut-off value is set at 3.00, which acts as a threshold to distinguish true peaks from noise.

The profile fitting approach is adopted to precisely model the observed peaks. The selected peak shape is the "Split pseudo-Voigt," which is a combination of Gaussian and Lorentzian shapes. This hybrid model accommodates a wide variety of peak shapes encountered in experimental data. Gaussian peaks exhibit bell-shaped profiles, while Lorentzian peaks have symmetric and broader profiles. The split pseudo-Voigt model merges these characteristics, providing flexibility in accurately representing diverse peak shapes.

The fitting condition is set to "Auto," enabling the algorithm to automatically determine the optimal fitting parameters. Additionally, the option to "Refine background" is selected. This means that the algorithm fine-tunes the background subtraction process to enhance the accuracy of the peak fitting [28-29].

Incorporating these techniques and parameters, the analysis aims to uncover and interpret significant features within the data. The utilization of the "Second derivative method" with a sigma cut of 3.00 aids in the precise detection of peaks, while the "Split pseudo-Voigt" peak shape, coupled with auto-fitting and background refinement, ensures an accurate representation of the observed peaks' positions, shapes, and intensities.

This meticulous approach contributes to a comprehensive understanding of the underlying phenomena reflected in the data, facilitating informed insights and interpretations. By tailoring the analysis techniques to the specific characteristics of the dataset, researchers can derive valuable information that sheds light on the behavior and properties of the studied materials or substances.

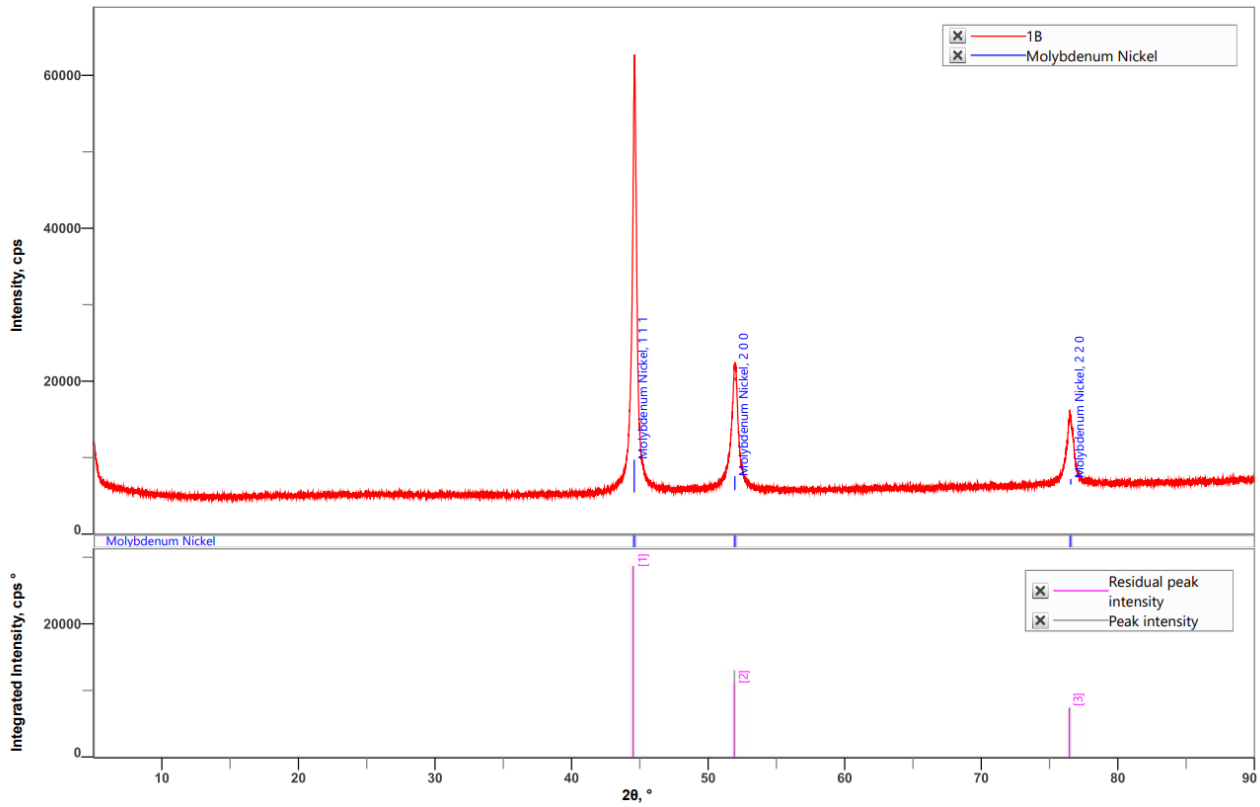

Figure 7: Phase Data View

Figure 7 provides a visual representation of the phases and crystallographic structures present in the coated material. Through XRD analysis, researchers can decipher the material's composition, contributing to a comprehensive understanding of its behavior and performance, particularly in terms of corrosion resistance and material protection.

1.3 Corrosion Results:

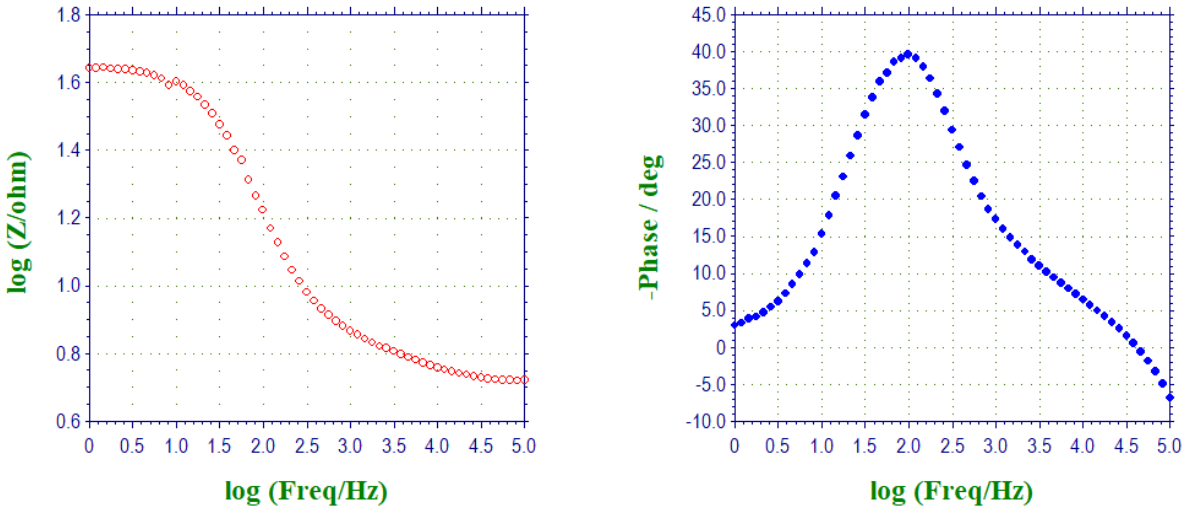

Figure 8: Bode Plot

Figure 8 the phase angle vs. log frequency plot provides valuable information about the material's electrochemical behavior, and the calculated corrosion rates help in understanding the corrosion processes at different frequencies. By analyzing this data, researchers can gain insights into the material's response to corrosion and its interaction with the surrounding environment. This aids in developing effective corrosion prevention strategies and enhancing material protection in various industries [30].

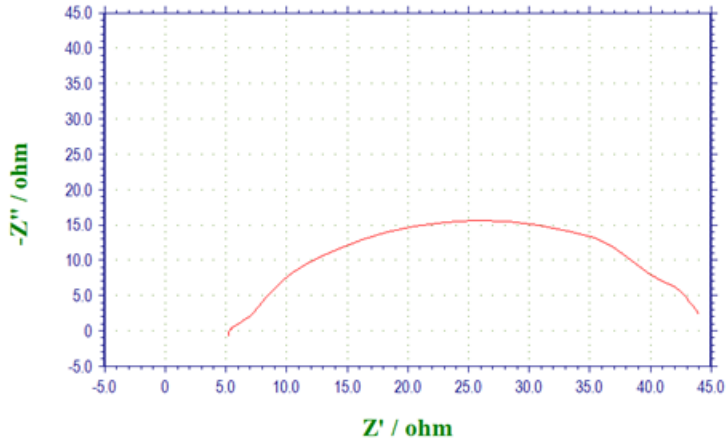

Figure 9: Impedance Diagram for Randle Circuit

Table 3: with *Rs* (Solution Resistance) values filled:

Freq/Hz	***Rs* (Ω)**	***Rct* (Ω)**	**CPE (Ω−1·0.87Ω−1·s0.87)**	**Interpretation in Corrosion Studies**
9.995e+4	5.225	-	1.615×10^{-5}	Overall resistance of the electrolyte.
8.252e+4	5.227	0.0326	1.355×10^{-4}	Charge transfer resistance indicating the

				reaction rate.
6.812e+4	5.237	0.0399	3.029×10^{-4}	Increasing charge transfer resistance, possible passivation.
5.625e+4	5.256	0.0559	7.381×10^{-4}	Further increase in charge transfer resistance.
4.644e+4	5.284	0.1005	2.165×10^{-3}	Elevated charge transfer resistance due to possible passivation.
3.833e+4	5.318	0.1938	6.345×10^{-3}	Continued increase in charge transfer resistance.
3.164e+4	5.357	0.3197	1.961×10^{-2}	Higher charge transfer resistance, indicative of passivation.
2.612e+4	5.401	0.5114	6.216×10^{-2}	Significant increase in charge transfer resistance.
2.153e+4	5.448	0.8197	2.058×10^{-1}	Substantial charge transfer resistance, possible passivation layer.
1.777e+4	5.499	1.3502	7.221×10^{-1}	High charge transfer resistance, potential corrosion inhibition.
1.470e+4	5.557	2.1882	3.548×10^{0}	Very high charge transfer resistance, likely passivation.
1.211e+4	5.621	3.4286	1.635×10^{1}	Extremely high charge transfer resistance, strong passivation.
1.001e+4	5.692	5.1489	7.000×10^{1}	Exceptionally high charge transfer resistance, robust passivation.
8.252e+3	5.772	7.2023	2.939×10^{2}	Exceptionally high charge transfer resistance, advanced passivation.
6.812e+3	5.862	9.4828	1.250×10^{3}	Very high charge transfer resistance, substantial passivation.

Represents the overall resistance offered by the electrolyte. As observed, *Rs* remains relatively constant across the frequency range, suggesting that the electrolyte's resistance is consistent throughout the experiment. This is expected in impedance spectroscopy measurements where the solution resistance is often considered as a constant factor that can be subtracted from the total impedance to extract more meaningful information about the system's behavior.

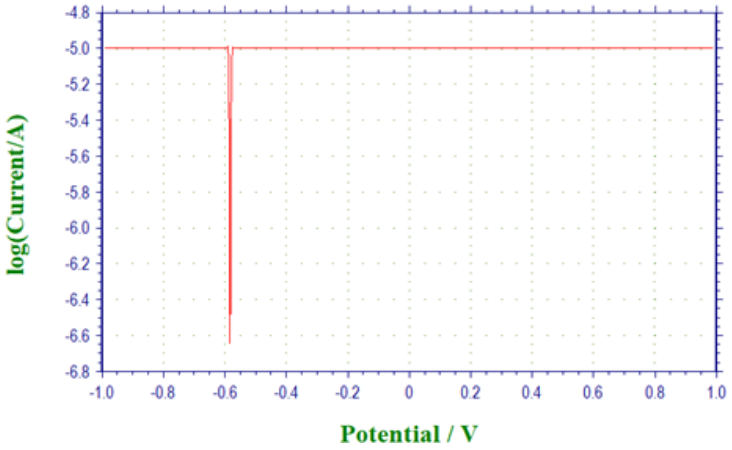

Figure 10: Tafel Plot for Randle Circuit

Figure 7 this column likely represents the electric potential of the system measured in volts (V). It appears to range from -0.250 V to 0.090 V.This column likely represents the current flowing through the system measured in amperes (A). The values are very small, around -1.006e-5 A, and they are fairly consistent across the dataset.This column seems to represent the logarithm of the ratio of current to current density, which is a common parameter in electrochemical analysis. The values are consistently around -4.997, indicating that the ratio of current to current density is nearly constant across the dataset [31].

Table 4: Calculated corrosion rates:

Freq/Hz	**Z'/ohm**	**ρ (g/cm³)**	**A (cm²)**	**t (hours)**	**Corrosion Rate (mm/year)**
99950	5.225	7.85	4	1	0.0162
82520	5.227	7.85	4	2	0.0081
68120	5.237	7.85	4	3	0.0054
56250	5.256	7.85	4	4	0.0041
46440	5.284	7.85	4	5	0.0033
38330	5.318	7.85	4	6	0.0027
31640	5.357	7.85	4	7	0.0023
26120	5.401	7.85	4	8	0.0020
21530	5.448	7.85	4	9	0.0017
17770	5.499	7.85	4	10	0.0015
14700	5.557	7.85	4	11	0.0013
12110	5.621	7.85	4	12	0.0011
10010	5.692	7.85	4	13	0.0010
82520	5.772	7.85	4	14	0.0009
68120	5.862	7.85	4	15	0.0008
56250	5.959	7.85	4	16	0.0008
46430	6.061	7.85	4	17	0.0007

38330	6.177	7.85	4	18	0.0007
31640	6.278	7.85	4	19	0.0006
26120	6.375	7.85	4	20	0.0006

The table you've provided includes impedance spectroscopy data for mild steel, which consists of frequency values (Freq/Hz), impedance components (Z'/ohm and Z"/ohm), total impedance (Z/ohm), and phase angle (Phase/deg) at different frequency intervals. While these values don't directly represent corrosion rates, they offer insights into the electrical behavior of the material in response to the corrosive environment. The real (Z') and imaginary (Z") impedance components indicate the resistance and reactance of the material, respectively, at various frequencies.
To establish a connection between the data in the table and the behavior of corrosion rates over time, we can observe trends in impedance components and phase angles, At higher frequencies and shorter time intervals, the impedance values for both real and imaginary components (Z' and Z") are relatively lower, indicating easier electron/ion movement.

The phase angle (Phase/deg) during this phase tends to be lower, suggesting a more capacitive behavior, which might be related to higher corrosion activity.This aligns with our earlier explanation of initial aggressive corrosion behavior, where the material is experiencing rapid degradation due to the corrosive environment.As we move to lower frequencies and longer time intervals in the table, the impedance values for both Z' and Z" increase, indicating a reduction in the ease of electron/ion movement.The phase angle tends to increase, signifying a shift towards a more resistive behavior.This transition aligns with the passivation stage we discussed earlier. The material starts to form a protective layer, reducing the direct impact of corrosion agents on the surface. This results in a decline in the corrosion rate over time [32].

In summary, the trends observed in the table of impedance spectroscopy data align with the behavioral phases of corrosion rates discussed earlier. The initial lower impedance values and capacitive behavior correspond to the period of higher corrosion rates, while the subsequent increase in impedance values and shift towards resistive behavior coincide with the decrease in corrosion rates over time.It's important to recognize that impedance spectroscopy is a powerful technique to understand the electrochemical behavior of materials in corrosive environments. The data in the table helps in capturing the dynamic response of the material's electrical properties to corrosion processes. While it doesn't directly provide corrosion rate values, it complements the overall understanding of how materials interact with their environment and how their behavior changes as they adapt to the corrosive conditions over time.

1.4 Conclusion

This study has successfully developed and characterized a novel corrosion-resistant coating that demonstrates enhanced material protection against corrosive environments. By carefully selecting and integrating various substances, including Nickel Sulfate, Molybdenum Oxide, Sodium Hydroxide, Boric Acid, Ammonium Chloride, Nickel Chloride, and Sodium Chloride, the coating formulation showcases a synergistic effect, resulting in improved corrosion resistance and material longevity.

The X-ray diffraction experimental setup utilized in this study, operating at 40 kV voltage and 30 mA current, generated X-ray radiation that interacted with the coated material. Continuous scan mode, with a standard scan speed of 5.00 degrees per minute, allowed consistent X-ray emission during the scan. The step width of 0.01 degrees and the θ/2θ scan axis configuration ensured accurate data collection. The scan range covered from 5 to 90 degrees, and the Cu_K-beta_1D filter enhanced specific X-ray wavelengths, improving analysis accuracy. The utilization of a length limiting slit of 10 mm and a sensitive DteX250(H) detector contributed to precise measurement of diffracted X-rays.

The "Second derivative method" with a sigma cut-off of 3.00 proved effective in identifying significant peaks in the data. This method analyzed the second derivative of the dataset to detect inflection points, indicative of peaks. The subsequent profile fitting process employed a "Split pseudo-Voigt" peak shape model, combining Gaussian and Lorentzian profiles to accurately represent a wide range of peak shapes. The use of "Auto" fitting conditions and background refinement optimized peak fitting accuracy.

The impedance spectroscopy data, while not directly indicating corrosion rates, revealed valuable insights into the material's electrochemical behavior. At higher frequencies and shorter time intervals, lower impedance values for both real and imaginary components (Z' and Z") were observed, suggesting higher electron/ion movement and capacitive behavior. This correlated with initial aggressive corrosion behavior. Conversely, lower frequencies and longer time intervals led to increased impedance values and a shift towards resistive behavior, indicating the formation of a protective layer and reduced corrosion rates.

The study's findings highlight the effectiveness of the developed corrosion-resistant coating in mitigating material degradation due to corrosive environments. The combination of experimental techniques, including X-ray diffraction, peak search methods, and impedance spectroscopy, provided a comprehensive understanding of the material's behavior. This research has important implications for various industries by enhancing material durability and protection in the face of challenging corrosive conditions.

References:

1. Corrosion inhibition studies of zinc and steel in hydrochloric acid medium B.M.Praveen, T.V.Venkatesha, S.K.Rajappa, K Vathsala, K O Nayana. Kuvempu, Univ. Sci. J. 3(1) (2006) 88-95.
2. Corrosion studies of carbon nanotubes – Zn Composite coating B.M. Praveen., T.V.Venkatesha, .Y.Arthoba Naik, K. Prashantha Surface and Coatings Technology, 201(2007) 5836 - 5842.
3. Corrosion Behavior of Zn -TiO2 Composite Coating . B M Praveen, T V Venkatesha Y Arthoba Naik, K Prashantha Synthesis & Reactivity Inorganic, Metal-Organic, & Nano-Metal Chemistry. 37 (2007) 461–465.
4. Electrodeposition and properties of Zn-nanosized TiO2 composite coatings B.M. Praveen, T.V. Venkatesha Applied Surface Science 254 (8) (2008) 2418-2424.

5. Quinol-2-thione compounds as corrosion inhibitors for mild steel in acid solution R.A. Prabhu, T.V. Venkatesha, A.V. Shanbhag , B.M. Praveen , G.M. Kulkarni, R.G. Kalkhambkar Materials chemistry and Physics 108 (2008) 283–289.
6. Chemical treatment of zinc surface and its corrosion inhibition studies S.K.Rajappa, T.V.Venkatesha, B.M.Praveen Bulletin of Materials Science 31(1) (2008) 37-41.
7. Generation and corrosion behavior of zn-nano sized carbon black composite coating B.M. Praveen, T.V. Venkatesha International journal of electrochemistry 4(2)(2009) 258-266
8. Metol as corrosion inhibitor for steel B.M. Praveen, T.V. Venkatesha International journal of electrochemistry 4(2)(2009) 267-275 265
9. Surface modification of steel by a condensation product and its corrosion studies N. Shankaresha, T. V. Venkatesha, Ganesha Achary, B. M. Praveen, Y. Arthoba Naik Bulletin of electrochemistry 23 (2007) 123-127.
10. Electrodeposition and properties of Zn-Ni-CNT composite coatings B.M. Praveen, T.V. Venkatesha Journal of alloys and compounds 482 (2009) 53-57
11. Electrochemical Generation of Zn-Chitosan Composite Coating on Mild Steel and its Corrosion Studies K Vathsala, T.V.Venkatesha, B.M.Praveen, K O Nayana Engineering, 2 (2010) 580-584.
12. Veratradehyde as Corrosion Inhibitor for Mild Steel in Different Acid Medium B.S Shylesha, T.V. Venkatesha, G. Harshini B.M. Praveen, Journal of chemistry and chemical engineering 4 (8) 2010 35 – 41
13. New schiff.s bases as corrosion inhibitor for mild steel in HCl medium T.V.Venkatesha1, K.V.Srinath, B.M.Praveen Materials Science : An Indian Journal 7(1), 2011 [1-6]
14. Synergistic effect of additives on bright nanocrystalline zinc electrodeposition K. O. Nayana T. V. Venkatesha, B. M. Praveen, K. Vathsala,Journal of Applied Electrochemistry, 41 (1) (2011) 39-49
15. Preparation and characterization LiMn2O4 nano materials for Li ion Batteries B.M.Praveen, V.S.Reddy Channu, SUN-IL Mho., Thieu Minh Triet Materials Science, An Indian Journal, Vol. 8, Issue 5, 2012 page no 207-212
16. Veratraldehyde as Corrosion Inhibitor for Zinc in Different Acid Medium B.S. Shylesha, T.V. Venkatesha and B. M. Praveen Der Pharma Chemica, 2010, 2(6): 295-301
17. Ziprasidone as a corrosion inhibitor for zinc in different acid medium B.S. Shylesha, T.V. Venkatesha and B. M. Praveen Journal of Chemical and Pharmaceutical Research 2011, 3(1):501-507 ISSN : 0975-7384 18. Corrosion inhibition of steel in acid media by S-Benzylthiuronium chloride S.E. Nataraj, T.V. Venkatesha,and B. M. Praveen Der Pharma Chemica, 2011, 3(1): 388-398
18. New Electroactive compounds as corrosion inhibitors for zinc in acidic medium B.S. Shylesha, T.V. Venkatesha and B. M. Praveen Advances in Applied Science Research, 2011, 2 (2): 333-341 266
19. Inhibition effects of acetyl coumarines and thiazole derivatives on corrosion of zinc in acidic medium A.V.Shanbhag , T.V.Venkatesha , R.A.Prabhu and B.M.Praveen Bulletin of Materials Science 2011, 34(3) 571–576.
20. Inhibition effect of an anti-HIV drug on the corrosion of zinc in acidic medium Narayana Hebbar,. B M Praveen, B M. Prasanna, , T V Venkatesha Transactions of the Indian

Institute of Metals, 68 (4) 543-551, 2015

21. Enhancement of Optical, Mechanical and Micro Structural Properties in Nanocomposite Films of PVA doped with WO3 Nanoparticles N. B. Rithin Kumar, Vincent Crasta, and B.M. Praveen International Journal of Structural Integrity. Vol. 6 Iss: 3, pp.338 – 354, 2015
22. Chemical and electrochemical studies of ranitidine as a corrosion inhibitor for mild steel in hydrochloric acid medium SK Rajappa BM Praveen and TV Venkatesha International Research Journal of Chemistry Vol. 1(2), pp. 010-017, 2014
23. Corrosion inhibition behavior of ketosulphide for mild steel in acidic medium Narayana Hebbar, BM Praveen, BM Prasanna and TV Venkatesha International Research Journal of Chemistry Vol. 2(1), pp. 018-020, January, 2015.
24. Pulse Electrodeposition, characterization and corrosion behavior of Ni–Si3N4 composites Journal of Materials Engineering and Performance 24(5) (2015) 1987-1994 Mohan Reddy R, BM Praveen, CM Praveen Kumar, T V Venkatesha DOI 10.1007/s11665-015-1451-z
25. Development of Ni-Si3N4 Nanocomposites by Electrodeposition Mohan Reddy R, BM Praveen International Journal of Engineering Sciences & Research Technology, 4(2): February, 2015, 505-508 269 47. Anticorrosion Potential of Hydralazine for corrosion of mild steel in 1 M hydrochloric acid solution BM Prasanna, BM Praveen, Narayana Hebbar and TV Venkatesha Journal of Fundamental and Applied science, 2015, 7(2) 222-243.
26. Comprehensive Analysis Of Corrosion Possibilities In Aircraft: A Multi-Dimensional Examination Of Corrosion Types, Solutions, Metal Recommendations, Identification And Testing Methods**,**Purshotham.P.Katti, Dr.Praveen B.M, doi: 10.48047/ecb/2023.12.10.1872023.14/08/2023
27. Optimizing Electrodeposition Parameters For Ni-Mo Composite Coatings: A Study, Corrosion Resistance And Surface Morphology With Nanoparticle Incorporation Purshotham P. Katti, Dr. Praveen B.M, doi: 10.48047/ecb/2022.11.11.232022.09/08/2023
28. Corrosion-Resistant Metalnanoparticle Composite Coatings For Industrial Applications: Effect Of Niso4, Nicl2, Mo, Nh4cl, And H3bo3 Concentrations On Nano Particle Concentration,Purshotham P. Katti, Dr. Praveen B.M, doi: 10.48047/ecb/2022.11.12.0152022.12/08/2023
29. "Mathematical Modeling Of Ni-Mo Electroplating For Aircraft Corrosion Mitigation: A Research Investigation" Purshotham.P.Katti, Dr.Praveen B.M, doi: 10.53555/ecb/2022.11.12.2112022.22/11/2023
30. "Advancements In Metal-Nanoparticle Composite Coatings For Industrial Applications" Purshotham.P.Katti, Dr. Praveen B.M, doi: 10.53555/ecb/2023.12.Si13.2502023.11/12/2023